ISSN 1070-3284, Russian Journal of Coordination Chemistry, 2021, Vol. 47, No. 4, pp. 280–295. © Pleiades Publishing, Ltd., 2021.
Russian Text © The Author(s), 2021, published in Koordinatsionnaya Khimiya, 2021, Vol. 47, No. 4, pp. 245–260.

Functionalized Trifluoromethyl-Containing Lithium β-Diketonate in the Synthesis of Homo- and Heteronuclear Complexes of Rare-Earth Metals

Yu. S. Kudyakova[a], P. A. Slepukhin[a], I. N. Ganebnykh[a], Ya. V. Burgart[a], V. I. Saloutin[a], and D. N. Bazhin[a, *]

[a] *Postovskii Institute of Organic Synthesis, Ural Branch, Russian Academy of Sciences, Yekaterinburg, Russia*
**e-mail: dnbazhin@gmail.com*

Received September 12, 2020; revised October 27, 2020; accepted October 29, 2020

Abstract—The reactions of functionalized lithium CF_3-β-diketonate (LiL) with trivalent rare-earth metal salts in methanol afford homobinuclear and heterobi(tri)nuclear complexes depending on the nature of the transition metal and anion (chlorides, nitrates, and acetates). In the cases of lanthanum(III) and cerium(III), homoleptic complexes $[(LnL_3)_2]$ are isolated (CIF files CCDC nos. 2031097 (**I*a***) and 2031102 (**I*b***)). The reaction of LiL with praseodymium(III) nitrate gives the new trimetallic structure $[(LiPrL_3)(LiL)(NO_3)(H_2O)_2]$ (CIF file CCDC no. 2031103 (**II**)), and the replacement of nitrate by chloride gives $[(PrL_3)(LiL)(H_2O)]$ (CIF file CCDC no. 2031104 (**III*a***)). Regardless of the nature of the anion of the salt in the series from neodymium(III) to ytterbium(III) and yttrium(III), Ln–Li β-diketonates $[(LnL_3)(LiL)(solv)]$ (solv is H_2O and MeOH) are formed, and their structures are characterized by X-ray structure analysis (CIF files CCDC nos. 2031099 (**III*b***), 2031100 (**III*c***), 2031098 (**IV*a***), 2031096 (**IV*c***), 2031094 (**IV*f***), 2031101 (**IV*g***), and 2031095 (**IV*h***)). The equilibrium of the diketonate isomeric forms in a solution of deuterated dimethyl sulfoxide is studied by ^{19}F NMR spectroscopy, and the qualitative composition of the polynuclear complexes is determined by mass spectrometry.

Keywords: β-diketonates, lanthanides, ^{19}F NMR spectroscopy, mass spectrometry

DOI: 10.1134/S1070328421040059

INTRODUCTION

β-Diketones represent a unique platform for the synthesis of metal-organic frameworks [1–4]. The formation of coordination compounds based on them with the majority of elements of the periodic table provides a possibility to produce new promising materials with a broad range of physicochemical properties, such as luminescence, [5–11], magnetic [12–16], and catalytic [17] properties. The synthesis of both mono- and polynuclear homo(hetero)metallic β-diketonates is a basic stage for further manufacturing oxide materials with a specified stoichiometric ratio of elements [18–24].

We have previously developed an approach to the synthesis of functionalized trifluorine-containing lithium diketonate (LiL), and on the basis of this approach we synthesized the heterobimetallic binuclear complexes $[(LnL_3)(LiL)(MeOH)]$ and $[(LnL_3)(LiL)(H_2O)]$ (Ln = Eu, Tb, and Dy) [25], $[LiLnL_4(H_2O)](CH_3CN)$ (Ln = Eu and Tb) [26], $M[TbL_4]$ (M = Na, K, and Cs) [27], and $(CuL_2)(Pb(Hfa)_2)$ [28], including those with promising (mechano)luminescence and magnetic properties. The methoxy groups in the α-position to the dicarbonyl fragment extends the coordination abilities of the diketonate anion for the synthesis of the bimetallic complexes, which was demonstrated by the coordination modes (**A** and **B**). The structure of the used β-diketonate anion L (Scheme 1a) and its coordination abilities (Scheme 1b) are presented below.

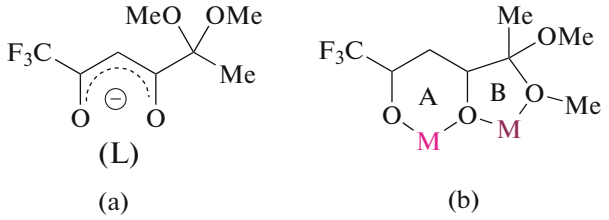

Scheme 1.

Under the action of strong Lewis acids, lithium diketonate LiL forms the furan derivative [29], which is a convenient building block for the synthesis of various heterocyclic systems, including bioactive compounds [30–34].

In this work, we studied the possibilities of functionalized lithium β-diketonate LiL in the synthesis of homo(hetero)metallic complexes, depending on the

nature of the rare-earth metal (REM) ion and inorganic anion.

EXPERIMENTAL

All procedures related to the synthesis of new complexes were carried out in air using commercial reagents ($LaCl_3·6H_2O$, $La(NO_3)_3·6H_2O$, $CeCl_3·6H_2O$, $PrCl_3·6H_2O$, $Pr(NO_3)_3·6H_2O$, $NdCl_3·6H_2O$, $SmCl_3·6H_2O$, $Gd(NO_3)_3·6H_2O$, $HoCl_3·6H_2O$, $Ho(OAc)_3·6H_2O$, $ErCl_3·6H_2O$, and $YbCl_3·6H_2O$ (purity of all salts not lower than 99.9%) and methanol (99%, Alfa Aesar). Trifluoromethyl-containing lithium β-diketonate LiL was synthesized using a described procedure [30]. Diketonates [$(LnL_3)(LiL)(MeOH)$] (**IV*b***, **IV*d***, and **IV*e***) were synthesized according to a published procedure [25].

The IR spectra of the compounds were recorded on a PerkinElmer Spectrum One FT-IR spectrometer in a range of 400–4000 cm^{-1} using a diffuse reflectance accessory (DRA) for solids. Elemental analyses were carried out on a PerkinElmer PE 2400 Series II automated analyzer. ^{19}F NMR spectra (376 MHz) were detected on a Bruker DRX-500 spectrometer (500 MHz) using C_6F_6 as an internal standard (δ_F = −162.9 ppm relative to $CFCl_3$).

The mass spectra of the complexes were recorded for solutions in methanol in the regime of positive ions in a mass range of 50–2800 Da on a MaXis Impact HD high-resolution quadrupole time-of-flight mass spectrometer (Bruker Daltonics) with the mounted standard source of electrospray ionization with syringe injection at a flow rate of 180 μL/h by the Tune_pos_-standard modified method. The mass scale was externally calibrated by a G1969-85000 standard mixture (Agilent Technologies). The data were collected and processed using the Bruker, version 1.7 and Compass DataAnalysis, version 4.2 program packages (Bruker). The calculated mass of the ion was presented on the basis of precise masses of the most abundant isotopes of the atoms of the ion, whereas the expected mass was obtained on the basis of the simulation mass spectrum from the instrumental resolution using the software of the mass spectrometer used.

Synthesis of complexes I–IV (general procedure). Lanthanide salt (0.5 mmol) was added to lithium β-diketonate LiL (2 mmol) in methanol (15 mL). The resulting suspension was heated to boiling and kept until a transparent solution was formed, after which the solution was cooled to room temperature and passed through the Celite® 545 layer. The slow evaporation of the solvent resulted in the formation of crystals of complex **IV**. In the cases of compounds **I–III**, the crystals were obtained by recrystallization from ethanol.

For $C_{48}H_{60}O_{24}F_{18}La_2$ (**I*a***)

Anal. calcd., %	C, 35.14	H, 3.69
Found, %	C, 34.91	H, 3.55

The yield was 220 mg (53%). Colorless crystals.

IR (DRA), ν, cm^{-1}: 3000, 2951, 2843 ν(C–H), 1682, 1632 ν(C=O), 1451, 1437 $\nu_{as}(CH_3)$, 1246–1139 ν(C–F). ^{19}F NMR ($(CD_3)_2SO$), δ, ppm: 88.1. ESI-MS: found 1647.1456 for $C_{48}H_{60}O_{24}F_{18}LiLa_2$ ($[La_2LiL_6]^+$), calculated 1647.1469, expected 1647.1470.

For $C_{48}H_{60}F_{18}O_{24}Ce_2$ (**I*b***)

Anal. calcd., %	C, 35.09	H, 3.68
Found, %	C, 34.78	H, 3.45

The yield was 178 mg (43%). Yellow crystals.

IR (DRA), ν, cm^{-1}: 3001, 2949, 2844 ν(C–H), 1680, 1633 ν(C=O), 1453, 1436 $\nu_{as}(CH_3)$, 1238–1142 ν(C–F). ^{19}F NMR ($(CD_3)_2SO$), δ, ppm: 89.5.

ESI-MS: found 1649.1454 for $C_{48}H_{60}O_{24}F_{18}LiCe_2$ ($[Ce_2LiL_6]^+$), calculated 1649.1450, expected 1659.1451.

For $C_{32}H_{44}NO_{21}F_{12}Li_2Pr$ (**II**)

Anal. calcd., %	C, 33.09	H, 3.82	N, 1.21
Found, %	C, 33.91	H, 3.65	N, 1.05

The yield was 464 mg (80%). Colorless crystals.

IR (DRA), ν, cm^{-1}: 3585–3493 ν(O–H), 2994–2845 ν(C–H), 1639 ν(C=O), 1488–1428 $\nu_{as}(CH_3)$, 1249–1140 ν(C–F). ^{19}F NMR ($(CD_3)_2SO$), δ, ppm: 87.7, 91.9 (in a ratio of 1 : 1.3). ESI-MS: found 1063.1507 for $C_{32}H_{40}O_{16}F_{12}Li_2Pr$ ($[PrLi_2L_4]^+$), calculated 1063.1516, expected 1063.1517.

For $C_{32}H_{42}F_{12}LiO_{17}Pr$ (**III*a***)

Anal. calcd., %	C, 35.77	H, 3.94
Found, %	C, 35.62	H, 3.77

The yield was 356 mg (66%). Blue crystals.

IR (DRA), ν, cm^{-1}: 3580–3496 ν(O–H), 2993–2844 ν(C–H), 1636 ν(C=O), 1486–1424 $\nu_{as}(CH_3)$, 1244–1139 ν(C–F). ^{19}F NMR ($(CD_3)_2SO$), δ, ppm: 88.0, 90.5, 91.6 (in a ratio of 1 : 0.4 : 5.8). ESI-MS: found

1063.1502 for $C_{32}H_{40}O_{16}F_{12}Li_2Pr$ ($[PrLiL_4]^+$), calculated 1063.1516, expected 1063.1517.

For $C_{32}H_{42}O_{17}F_{12}LiNd$ (**III*b***)

Anal. calcd., %	C, 35.66	H, 3.93
Found, %	C, 35.44	H, 3.75

The yield was 210 mg (39%). Blue crystals.

IR (DRA), ν, cm^{-1}: 3585–3494 ν(O–H), 2989–2846 ν(C–H), 1636 ν(C=O), 1481–1422 $\nu_{as}(CH_3)$, 1242–1140 ν(C–F). ^{19}F NMR ($(CD_3)_2SO$), δ, ppm: 87.8, 89.9, 90.5 (in a ratio of 1 : 0.25 : 3). ESI-MS: found 1064.1503 for $C_{32}H_{42}O_{17}F_{12}Li_2Nd$ ($[NdLi_2L_4]^+$), calculated 1064.1517, expected 1064.1519.

For $C_{32}H_{42}F_{12}LiO_{17}Y$ (**III*c***)

Anal. calcd., %	C, 37.59	H, 4.14
Found, %	C, 37.32	H, 3.98

The yield was 256 mg (50%). Colorless crystals.

IR (DRA), ν, cm^{-1}: 3587–3496 ν(O–H), 2993–2848 ν(C–H), 1637 ν(C=O), 1483–1419 $\nu_{as}(CH_3)$, 1240–1137 ν(C–F). ^{19}F NMR ($(CD_3)_2SO$), δ, ppm: 87.8, 87.9 (in a ratio of 1 : 0.23). ESI-MS: found 1011.1498 for $C_{32}H_{40}O_{16}F_{12}Li_2Y$ ($[YLi_2L_4]^+$), calculated 1011.1498, expected 1011.1499.

For $C_{32}H_{42}O_{17}F_{12}LiSm$ (**IV*a***)

Anal. calcd., %	C, 36.10	H, 4.04
Found, %	C, 35.84	H, 3.87

IR (DRA), ν, cm^{-1}: 3539–3489 ν(O–H), 3002–2840 ν(C–H), 1632 ν(C=O), 1463–1436 $\nu_{as}(CH_3)$, 1189–1143 ν(C–F). ^{19}F NMR ($(CD_3)_2SO$), δ, ppm: 87.7, 88.1 (in a ratio of 1 : 2.9). ESI-MS: found 1074.1636 for $C_{32}H_{40}O_{16}F_{12}Li_2Sm$ ($[SmLi_2L_4]^+$), calculated 1074.1637, expected 1074.1639.

For $C_{33}H_{44}O_{17}F_{12}LiEu$ (**IV*b***)

Anal. calcd., %	C, 36.05	H, 4.03
Found, %	C, 35.64	H, 3.83

IR (DRA), ν, cm^{-1}: 3694, 3395 ν(O–H), 2949, 2841 ν(C–H), 1634 ν(C=O), 1519, 1473, 1435 $\nu_{as}(CH_3)$, 1187, 1139 ν(C–F). ^{19}F NMR ($(CD_3)_2SO$), δ, ppm: 84.2, 84.9, 87.8 (in a ratio of 7 : 1 : 3). ESI-MS: found 1075.1646 for $C_{32}H_{40}O_{16}F_{12}Li_2Eu$ ($[EuLi_2L_4]^+$), calculated 1075.1652, expected 1076.1656.

For $C_{32}H_{42}O_{17}F_{12}LiGd$ (**IV*c***)

Anal. calcd., %	C, 35.87	H, 4.01
Found, %	C, 35.81	H, 3.88

The yield was 312 mg (57%). Colorless crystals.

IR (DRA), ν, cm^{-1}: 3695 ν(O–H), 2997–2841 ν(C–H), 1635 ν(C=O), 1475–1436 $\nu_{as}(CH_3)$, 1188–1136 ν(C–F). ^{19}F NMR ($(CD_3)_2SO$; δ, ppm: 75.9–86.3, 87.7 (in a ratio of 1.3 : 1). ESI-MS: found 1080.1694 for $C_{32}H_{40}O_{16}F_{12}Li_2Gd$ ($[GdLi_2L_4]^+$), calculated 1080.1680, expected 1080.1690.

For $C_{33}H_{44}O_{17}F_{12}LiTb$ (**IV*d***)

Anal. calcd., %	C, 36.63	H, 3.79
Found, %	C, 35.82	H, 4.01

IR (DRA), ν, cm^{-1}: 3695, 3387 ν(O–H), 2950, 2841 ν(C–H), 1635 ν(C=O), 1519, 1476 s, 1437 $\nu_{as}(CH_3)$, 1188, 1141 ν(C–F). ^{19}F NMR ($(CD_3)_2SO$), δ, ppm: 87.8, 111.5, 117.7 (in a ratio of 3 : 1 : 9). ESI-MS: found 1081.1685 for $C_{32}H_{40}O_{16}F_{12}Li_2Tb$ ($[TbLi_2L_4]^+$), calculated 1081.1693, expected 1081.1694.

For $C_{33}H_{44}O_{17}F_{12}LiDy$ (**IV*e***)

Anal. calcd., %	C, 35.49	H, 3.84
Found, %	C, 35.70	H, 4.00

IR (DRA), ν, cm^{-1}: 3695, 3383 ν(O–H), 2949, 2841 ν(C–H), 1635 ν(C=O), 1518, 1476 s, 1435 $\nu_{as}(CH_3)$, 1186, 1139 ν(C–F). ^{19}F NMR ($(CD_3)_2SO$), δ, ppm: 87.7, 106.1, 120.2 (in a ratio of 2 : 1 : 6). ESI-MS: found 1086.1736 for $C_{32}H_{40}O_{16}F_{12}Li_2Dy$ ($[DyLi_2L_4]^+$), calculated 1086.1731, expected 1086.1741.

For $C_{32}H_{42}O_{17}F_{12}LiHo$ (**IV*f***)

Anal. calcd., %	C, 35.63	H, 3.99
Found, %	C, 35.44	H, 3.79

The yield was 410 mg (74%). Colorless crystals.

IR (DRA), ν, cm^{-1}: 3695 ν(O–H), 2996–2841 ν(C–H), 1634 ν(C=O), 1477–1436 $\nu_{as}(CH_3)$, 1185–1137 ν(C–F). ^{19}F NMR ($(CD_3)_2SO$), δ, ppm: 87.7, 96.2, 102.1 (in a ratio of 1 : 0.5 : 2.1). ESI-MS: found 1087.1735 for $C_{32}H_{40}O_{16}F_{12}Li_2Ho$ $[HoLi_2L_4]^+$, calculated 1087.1743, expected 1087.1744.

For $C_{32}H_{42}O_{17}F_{12}LiEr$ (**IV*g***)

Anal. calcd., %	C, 35.55	H, 3.98
Found, %	C, 35.39	H, 3.81

The yield was 423 mg (76%). Colorless crystals.

IR (DRA), ν, cm^{-1}: 3692 ν(O–H), 2995–2840 ν(C–H), 1635 ν(C=O), 1474–1435 $\nu_{as}(CH_3)$, 1183–1138 ν(C–F). ^{19}F NMR ($(CD_3)_2SO$), δ, ppm: 71.5, 72.6, 87.7 (in a ratio of 1 : 0.3 : 0.4). ESI-MS: found

1088.1704 for $C_{32}H_{40}O_{16}F_{12}Li_2Er$ ($[ErLi_2L_4]^+$), calculated 1088.1742, expected 1088.1745.

For $C_{32}H_{42}O_{17}F_{12}LiYb$ (**IV*h***)		
Anal. calcd., %	C, 35.57	H, 3.96
Found, %	C, 35.41	H, 3.78

The yield was 413 mg (74%). Colorless crystals.

IR (DRA), ν, cm^{-1}: 3636 ν(O–H), 2997–2841 ν(C–H), 1639 ν(C=O), 1479–1437 $\nu_{as}(CH_3)$, 1202–1133 ν(C–F). ^{19}F NMR ($(CD_3)_2SO$), δ, ppm: 78.6, 81.1, 87.8 (in a ratio of 1 : 0.3 : 0.5). ESI-MS: found 1096.1824 for $C_{32}H_{40}O_{16}F_{12}Li_2Yb$ ($[YbLi_2L_4]^+$), calculated 1096.1828, expected 1096.1835.

X-ray structure analysis (XSA). The crystallographic data for single crystals of complexes **I**–**IV** were obtained on an Xcalibur 3 automated four-circle diffractometer with a CCD detector using a standard procedure (MoK_α radiation, graphite monochromator, ω scan mode with an increment of 1° at $T = 295(2)$ K). An empirical absorption correction was applied. The structures were determined by direct statistical methods and refined by full-matrix least squares for F^2 in the anisotropic approximation for all non-hydrogen atoms. Hydrogen atoms were placed in the geometrically calculated positions and refined by the riding model. All calculations were performed in the Olex program shell [35] using the SHELX program package [36]. The shape of the coordination polyhedra [LnOx] was calculated using the SHAPE program [37, 38]. The crystallographic data and structure refinement parameters and details for compounds **I**–**IV** are presented in Table 1.

The coordinates of atoms and other structural parameters for compounds **I**–**IV** were deposited with the Cambridge Crystallographic Data Centre (CIF files CCDC nos. 2031097 (**I*a***), 2031102 (**I*b***), 2031103 (**II**), 2031104 (**III*a***), 2031099 (**III*b***), 2031100 (**III*c***), 2031098 (**IV*a***), 2031096 (**IV*c***), 2031094 (**IV*f***), 2031101 (**IV*g***), and 2031095 (**IV*h***); deposit@ccdc.cam.ac.uk or http://www.ccdc.cam.ac.uk/data_request/cif).

RESULTS AND DISCUSSION

When using REM in the reactions with lithium CF_3-β-diketonate LiL, various heterometallic structures were synthesized, depending on the metal ion nature and, in some cases, on the anion nature (Table 2). The homoleptic complexes $[(LnL_3)_2]$ are formed (**I*a*** and **I*b***, Scheme 2) in the reactions of lanthanum(III) and cerium(III) chlorides and nitrates with LiL. Two types of diketonates were isolated in the reactions of LiL with praseodymium(III) salts, $[(LiPrL_3)(LiL)(NO_3)(H_2O)_2]$ (**II**) and $[(PrL_3)(LiL)(H_2O)]$ (**III*a***), depending on the nature of the anion used (Scheme 2).

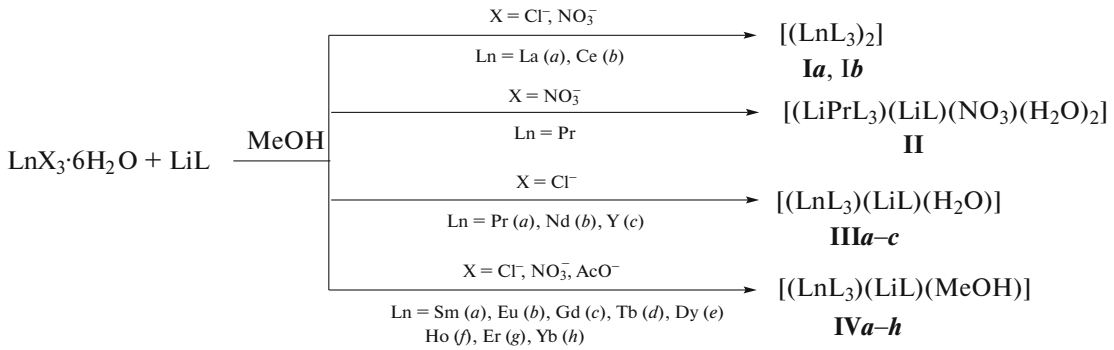

Scheme 2.

The reactions of trivalent metal salts (chlorides, nitrates, or acetates) in the series from neodymium(III) to ytterbium(III) were found to result in the formation of the structures $[(PrL_3)(LiL)(solv)]$ (**III*b***, **IV*a***, **IV*c***, and **IV*f***–**IV*h***) (Ln = Nd, Sm, Hd, Ho, Er, and Yb) (Scheme 2) similar to the earlier described bimetallic diketonates Ln–Li (**IV*b***, **IV*d***, and **IV*e***) (Ln = Tb(III), Eu(III), and Dy(III)) [24]. The majority of the lanthanides used form heteronuclear complexes **IV*a***–**IV*h*** with the MeOH molecule as a coligand, and only complex **III*b*** with the Nd(III) ion, whose radius is commensurable with that of the Pr(III) ion, contains the water molecule. Among REM, yttrium(III) chloride gives the $[(YL_3)(LiL)(H_2O)]$ complex (**III*c***) similarly to the main series of lanthanides from praseodymium to ytterbium.

In all synthesized complexes with the REM ions, Ln(III) forms the tris(diketonate) fragment. The further saturation of coordination possibilities of the metal ion depends on its radius.

In the cases of complexes **I*a*** and **I*b*** (lanthanum(III) and cerium(III)) characterized by the largest ion radii among trivalent REM ions, two tris(diketonate) fragments form neutral binuclear structures **I*a*** and **I*b*** without additional coligands (Fig. 1a). According to the XSA data, the oxygen atoms of the methoxy

Table 1. Selected crystallographic characteristics and experimental XSA parameters for complexes **I**–**IV**

Parameter	Value					
	I*a*	**I*b***	**II**	**III*a***	**III*b***	**III*c***
Empirical formula	$C_{48}H_{60}O_{24}F_{18}La_2$	$C_{48}H_{60}O_{24}F_{18}Ce_2$	$C_{32}H_{44}NO_{21}F_{12}Li_2Pr$	$C_{32}H_{42}O_{17}F_{12}LiPr$	$C_{32}H_{42}O_{17}F_{12}LiNd$	$C_{32}H_{42}O_{17}F_{12}LiY$
FW	1640.78	1643.20	1161.47	1074.51	1077.84	1022.51
Temperature, K	295(2)					
Crystal system	Monoclinic					
Space group	$P2_1/c$		$C2/c$	$P2_1/c$	$P2_1/c$	$P2_1/c$
Cell parameters:						
a, Å	13.3363(6)	13.3713(4)	39.816(2)	17.0662(6)	17.0444(8)	17.1022(13)
b, Å	21.0621(11)	21.1070(8)	12.6508(6)	12.0958(5)	12.0918(7)	11.9268(7)
c, Å	24.0099(11)	24.0242(10)	24.3826(13)	22.5016(10)	22.4600(12)	22.110(2)
β, deg	101.507(4)	101.643(4)	125.243(5)	94.515(3)	94.352(5)	94.052(8)
V, Å^3	6608.6(5)	6640.8(4)	10030.4(11)	4630.6(3)	4615.6(4)	4498.5(6)
Z	4	4	8	4	4	4
ρ_{calc}, g cm^{-3}	1.649	1.644	1.5381	1.5412	1.551	1.510
μ, mm^{-1}	1.398	1.476	1.086	1.163	1.236	1.411
Crystal size, mm	0.43 × 0.31 × 0.26	0.45 × 0.37 × 0.29	0.35 × 0.30 × 0.25	0.48 × 0.39 × 0.26	0.42 × 0.33 × 0.25	0.43 × 0.36 × 0.29
θ_{min}–θ_{max}, deg	3.42–30.92	3.42–30.89	3.52–26.37	3.49–30.87	3.49–30.93	3.53–27.10
F(000)	3264	3272	4675.3662	2161.5076	2164	2080
R_{int}	0.0530	0.0631	0.0792	0.0486	0.0447	0.0627
Ranges of reflection indices	$-17 \le h \le 17$ $-24 \le k \le 29$ $-32 \le l \le 34$	$-18 \le h \le 19$ $-30 \le k \le 29$ $-33 \le l \le 31$	$-49 \le h \le 49$ $-15 \le k \le 15$ $-30 \le l \le 30$	$-22 \le h \le 23$ $-17 \le k \le 15$ $-31 \le l \le 18$	$-23 \le h \le 20$ $-17 \le k \le 16$ $-30 \le l \le 31$	$-21 \le h \le 21$ $-9 \le k \le 15$ $-28 \le l \le 28$
Measured reflections	44263	44623	30223	32354	32059	27912
Independent reflections	17871	17557	10230	12560	12417	9802
Number of reflections with $I > 2\sigma(I)$	10014	9717	6882	7481	7945	5614
GOOF	1.012	1.002	1.019292	1.085404	1.027	1.008
R factors for $F^2 > 2\sigma(F^2)$	$R_1 = 0.0603$ $wR_2 = 0.1429$	$R_1 = 0.0594$ $wR_2 = 0.1360$	$R_1 = 0.0510$	$R_1 = 0.0666$	$R_1 = 0.00578$ $wR_2 = 0.1579$	$R_1 = 0.0558$ $wR_2 = 0.1112$
R factors for all reflections	$R_1 = 0.1194$ $wR_2 = 0.1925$	$R_1 = 0.1185$ $wR_2 = 0.1917$	$R_1 = 0.0834$ $wR_2 = 0.1368$	$R_1 = 0.1132$ $wR_2 = 0.2471$	$R_1 = 0.0987$ $wR_2 = 0.2089$	$R_1 = 0.1216$ $wR_2 = 0.1439$
Residual electron density (max/min), e/Å^3	1.305/–1.734	1.531/–1.854	0.964225/–1.172986	1.459/–1.925	1.069/–1.790	0.738/–0.508

Table 1. (Contd.)

Parameter	Value				
	IV*a*	**IV*c***	**IV*f***	**IV*g***	**IV*h***
Empirical formula	$C_{33}H_{44}F_{12}O_{17}LiSm$	$C_{33}H_{44}O_{17}F_{12}LiGd$	$C_{33}H_{44}O_{17}F_{12}LiHo$	$C_{33}H_{44}O_{17}F_{12}LiEr$	$C_{33}H_{44}O_{17}F_{12}LiYb$
FW	1097.97	1104.87	1112.55	1114.88	1120.66
Temperature, K	295(2)				
Crystal system	Monoclinic				
Space group	*Pn*				
Cell parameters:					
a, Å	12.3045(4)	12.2645(5)	12.3093(4)	12.3233(7)	12.2414(5)
b, Å	12.2281(3)	12.2046(6)	12.1904(3)	12.2192(6)	12.1590(4)
c, Å	15.9129(5)	15.8864(7)	15.8189(4)	15.8767(9)	15.8128(4)
β, deg	94.840(3)	94.702(4)	94.475(3)	94.374(5)	94.475(3)
V, Å^3	2385.72(12)	2369.93(18)	2366.47(12)	2383.8(2)	2346.45(13)
Z	2	2	2	2	2
ρ_{calc}, g cm^{-3}	1.528	1.548	1.561	1.553	1.586
μ, mm^{-1}	1.340	1.509	1.782	1.869	2.104
Crystal size, mm	0.44 × 0.38 × 0.27	0.35 × 0.30 × 0.25	0.44 × 0.38 × 0.31	0.44 × 0.39 × 0.31	0.41 × 0.36 × 0.32
θ_{min}–θ_{max}, deg	3.571–30.803	2.11–30.90	2.58–29.44	2.58–29.44	3.599–30.903
F(000)	1102	1106	1112	1114	1118
R_{int}	0.0418	0.0254	0.0387	0.0456	0.0403
Ranges of reflection indices	$-17 \le h \le 16$ $-17 \le k \le 17$ $-22 \le l \le 20$	$-17 \le h \le 14$ $-8 \le k \le 17$ $-18 \le l \le 21$	$-16 \le h \le 15$ $-16 \le k \le 16$ $-21 \le l \le 21$	$-17 \le h \le 16$ $-17 \le k \le 9$ $-21 \le l \le 21$	$-17 \le h \le 17$ $-16 \le k \le 17$ $-13 \le l \le 22$
Measured reflections	31117	12931	28710	15810	19345
Independent reflections	11804	8011	10471	9220	7970
Number of reflections with $I > 2\sigma(I)$	9522	6991	9621	7020	6329
GOOF	1.025	1.004	1.010	1.030	1.043
R factors	$R_1 = 0.0475$	$R_1 = 0.0385$	$R_1 = 0.0336$	$R_1 = 0.0539$	$R_1 = 0.0467$
for $F^2 > 2\sigma(F^2)$	$wR_2 = 0.1254$	$wR_2 = 0.0960$	$wR_2 = 0.0882$	$wR_2 = 0.1372$	$wR_2 = 0.1242$
R factors	$R_1 = 0.0661$	$R_1 = 0.0479$	$R_1 = 0.0385$	$R_1 = 0.0780$	$R_1 = 0.0651$
for all reflections	$wR_2 = 0.1585$	$wR_2 = 0.0960$	$wR_2 = 0.0951$	$wR_2 = 0.1742$	$wR_2 = 0.1572$
Residual electron density (max/min), e/Å^3	1.193/–1.546	0.816/–0.722	1.509/–0.935	1.646/–2.414	1.315/–1.558

Table 2. Selected geometric characteristics of the series of heterometallic Ln–Li diketonates

Composition of complex	Distance, Å				Geometry of $[LnO_n]$*	Literature
	Ln–O	Ln–μ_2-O	Ln···Ln	Ln···Li*		
$[(LaL_3)_2]$ (**I*a***)	2.421–2.800	2.561–2.759	3.807 10.039		JSPC-10	
$[(CeL_3)_2]$ (**I*b***)	2.417–2.804	2.547–2.725	3.785 10.104		JSPC-10	
$[(LiPrL_3)(LiL)(NO_3)(H_2O)_2]$ (**II**)	2.438–2.468	2.497–2.709	10.219	3.570 3.639	JSPC-10	
$[(PrL_3)(LiL)(H_2O)]$ (**III*a***)	2.399–2.559	2.419–2.457	9.610	3.564	TDD-8	
$[(NdL_3)(LiL)(H_2O)]$ (**III*b***)	2.392–2.554	2.404–2.448	9.618	3.536	TDD-8	
$[(YL_3)(LiL)(H_2O)]$ (**III*c***)	2.302–2.480	2.305–2.376	9.630	3.469	TDD-8	
$[(SmL_3)(LiL)(MeOH)]$ (**IV*a***)	2.351–2.556	2.384–2.443	10.557	3.505	TDD-8	
$[(EuL_3)(LiL)(MeOH)]$	2.334–2.533	2.362–2.426	10.527	3.498	TDD-8	25
$[(EuL_3)(LiL)(H_2O)]$	2.346–2.523	2.361–2.412	9.613	3.508	TDD-8	25
$[LiEuL_4(H_2O)](CH_3CN)$	2.352–2.389	2.420–2.461	9.560	3.568	BTPR-8	26
$[(GdL_3)(LiL)(MeOH)]$ (**IV*c***)	2.322–2.529	2.361–2.411	10.564	3.479	TDD-8	
$[(TbL_3)(LiL)(MeOH)]$	2.306–2.505	2.350–2.404	10.552	3.471	TDD-8	25
$[(TbL_3)(LiL)(H_2O)]$	2.320–2.503	2.330–2.389	9.923	3.494	TDD-8	25
$[LiTbL_4(H_2O)](CH_3CN)$	2.344–2.368	2.398–2.448	9.545	3.535	BTPR-8	26
$[(DyL_3)(LiL)(MeOH)]$	2.298–2.504	2.340–2.395	10.615	3.452	TDD-8	25
$[(DyL_3)(LiL)(H_2O)]$	2.311–2.496	2.321–2.383	9.633	3.482	TDD-8	25
$[(HoL_3)(LiL)(MeOH)]$ (**IV*f***)	2.289–2.489	2.322–2.381	10.597	3.455	TDD-8	
$[(ErL_3)(LiL)(MeOH)]$ (**IV*g***)	2.298–2.501	2.300–2.355	10.643	3.457	TDD-8	
$[(YbL_3)(LiL)(MeOH)]$ (**IV*h***)	2.270–2.476	2.260–2.350	10.591	3.439	TDD-8	

* According to the data calculated data using the SHAPE program (JSPC-10 is clinocrown, TDD-8 is trigonal dodecahedron, BTPR-8 is bicapped trigonal prism, and SAPR-8 is square antiprism).

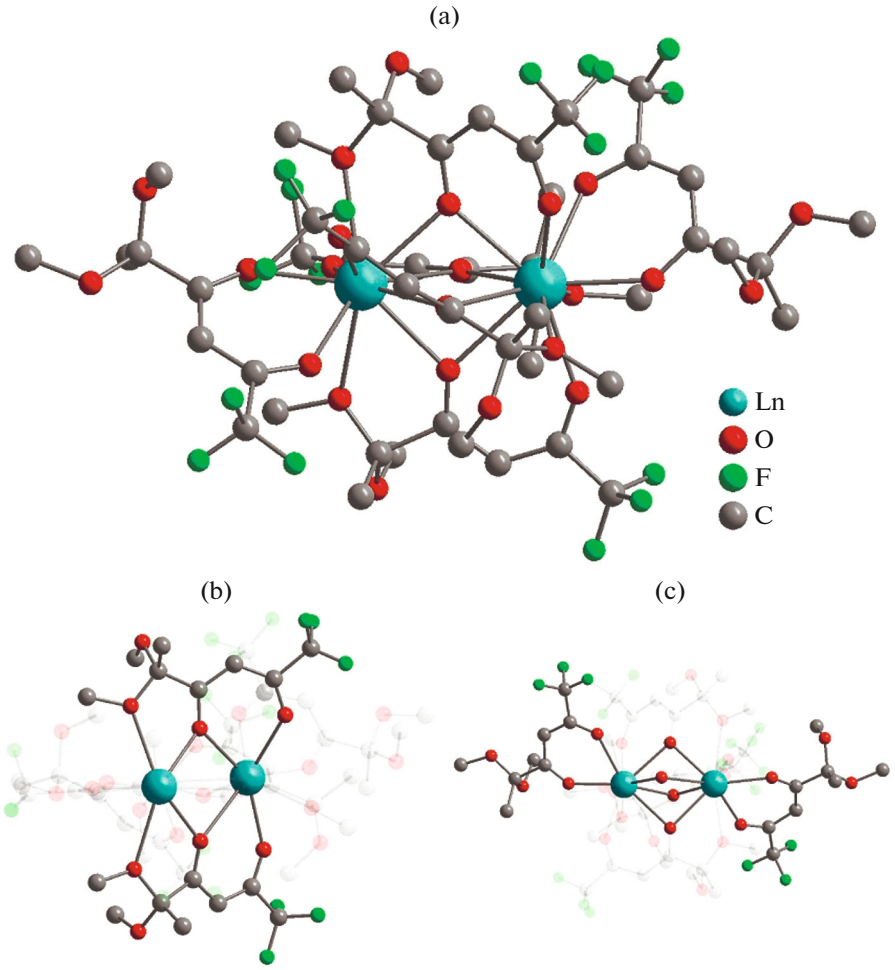

Fig. 1. (a) Molecular structures of complexes **I*a*** (Ln = La) and **I*b*** (Ln = Ce) (hydrogen atoms are omitted), (b) organization of the bimetallic framework involving two diketonate anions with bridging oxygen atoms, and (c) two diketonates not involved in the additional coordination.

substituent and carbonyl group adjacent to the acetal fragment of the ligand (coordination mode B, Scheme 1b) act as bridging heteroatoms between two Ln(III) ions (Fig. 1b). In each tris(diketonate) fragment, one of the ligand molecules forms the six-membered metallocycle via mode A (Fig. 1c). Unlike the binuclear $[Ln(dpm)_3]_2$ complexes synthesized from dipivaloylmethane with heptacoordinated lanthanide ions [21, 39, 40], in compounds **I*a*** and **I*b*** the coordination environment of 4*f*-metal ions includes ten oxygen atoms of the ligands. Two polyhedra $[LnO_{10}]$ have the common face of four bridging oxygen atoms of diketonates and are described most precisely by the clinocrown geometry (Table 2, Fig. 2a). The intramolecular Ln...Ln distance is 3.8066(4) and 3.7853(4) Å for complexes **I*a*** and **I*b***, respectively. For comparison, the analogous La...La parameter for the $[La(dpm)_3]_2$ complex is 4.1028(5) Å [34]. Thus, the involvement of additional coordination oxygen atoms of the methoxy groups of the ligand decreases the distance between the lanthanide atoms. The range of Ln...O bond lengths in the tris(diketonate) fragment is 2.4214–2.8001 Å, which is comparable with the values detected for the bonds of lanthanide with the bridging oxygen atoms ranging from 2.5607 to 2.7293 Å. In the crystal packings of compounds **I*a*** and **I*b***, the bimetallic frameworks of the molecules are oriented along the *a* axis (Fig. 3).

According to the XRD data, complex **II** has a more complicated structure. The trimetallic structure of compound **II** containing the decacoordinated praseodymium(III) ion and two lithium atoms is formed due to the coordination of four diketonate anions (Fig. 4a). One of the ligands of the tris(diketonate) fragment is involved in the chelation of the lithium atom of the initial LiL molecule (Fig. 4b). The coordination environment of the praseodymium ion in compound **II** is saturated due to the nitrate anion, three diketonate

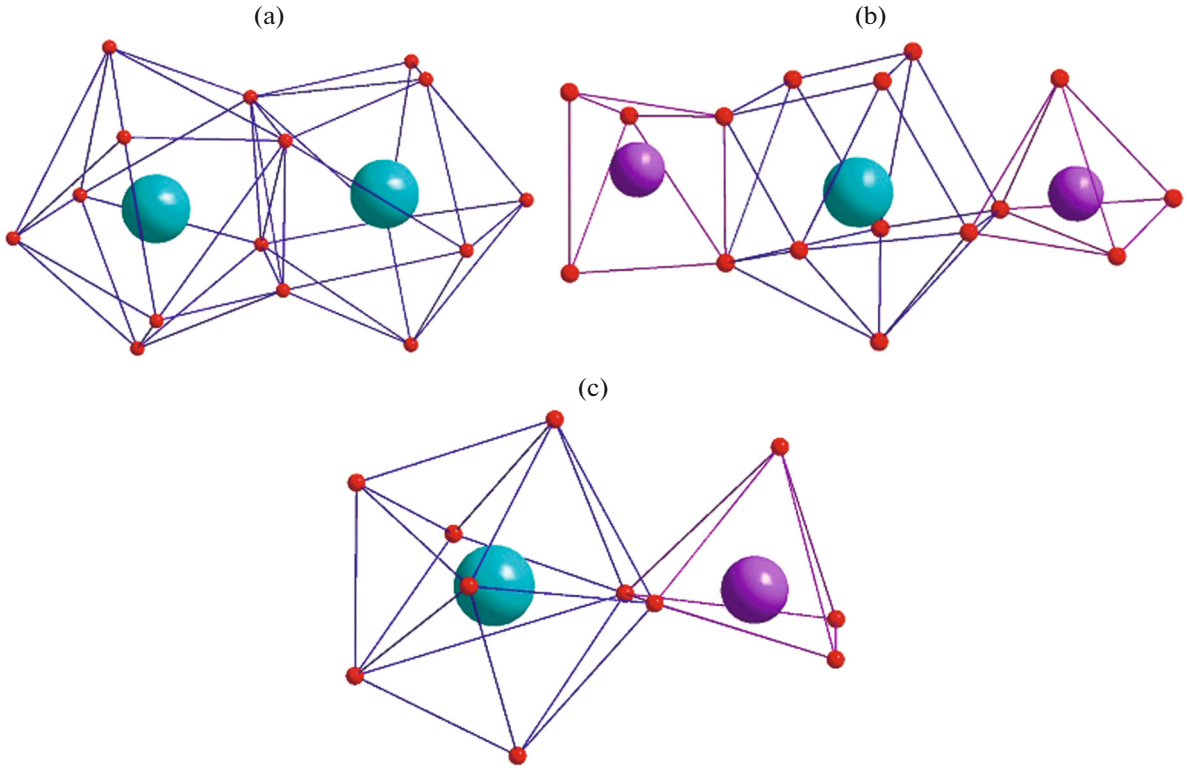

Fig. 2. Geometries of (a) coordination polyhedra LnO_x ($x = 8$, 10) and LiO_5 in homoleptic complexes **I*a*** and **I*b***, (b) trimetallic diketonate **II**, and (c) binuclear compounds **III*a*–III*c*** and **IV*a*–IV*h***.

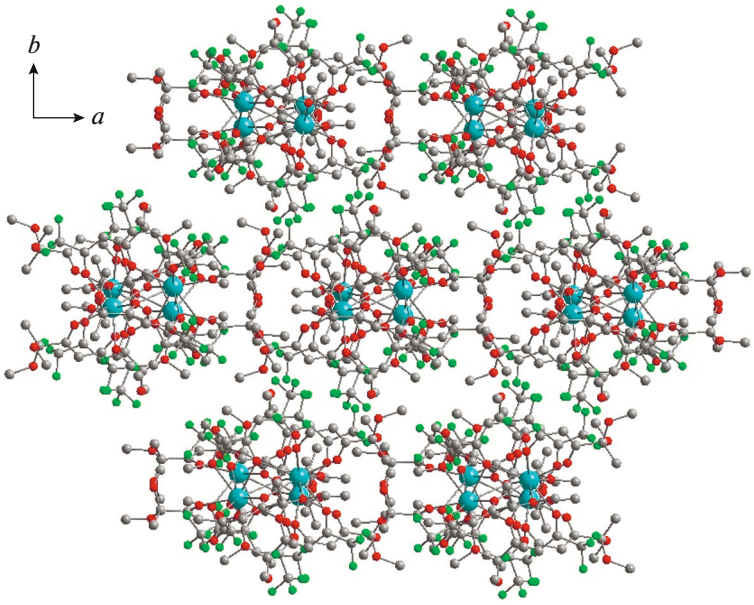

Fig. 3. Molecular packings of complexes **I*a*** and **I*b*** along the *c* axis (hydrogen atoms are omitted).

anions (coordination mode A, Fig. 4c), one methoxy group, and the bridging oxygen atom of the dicarbonyl fragment LiL (coordination mode B, Fig. 4b). The unusual structure of complex **II** includes the second lithium ion, whose coordination also occurs due to four oxygen atoms of two diketonate molecules (methoxy groups and oxygen of the diketonate fragment, coordination mode B) (Fig. 4c). The distance

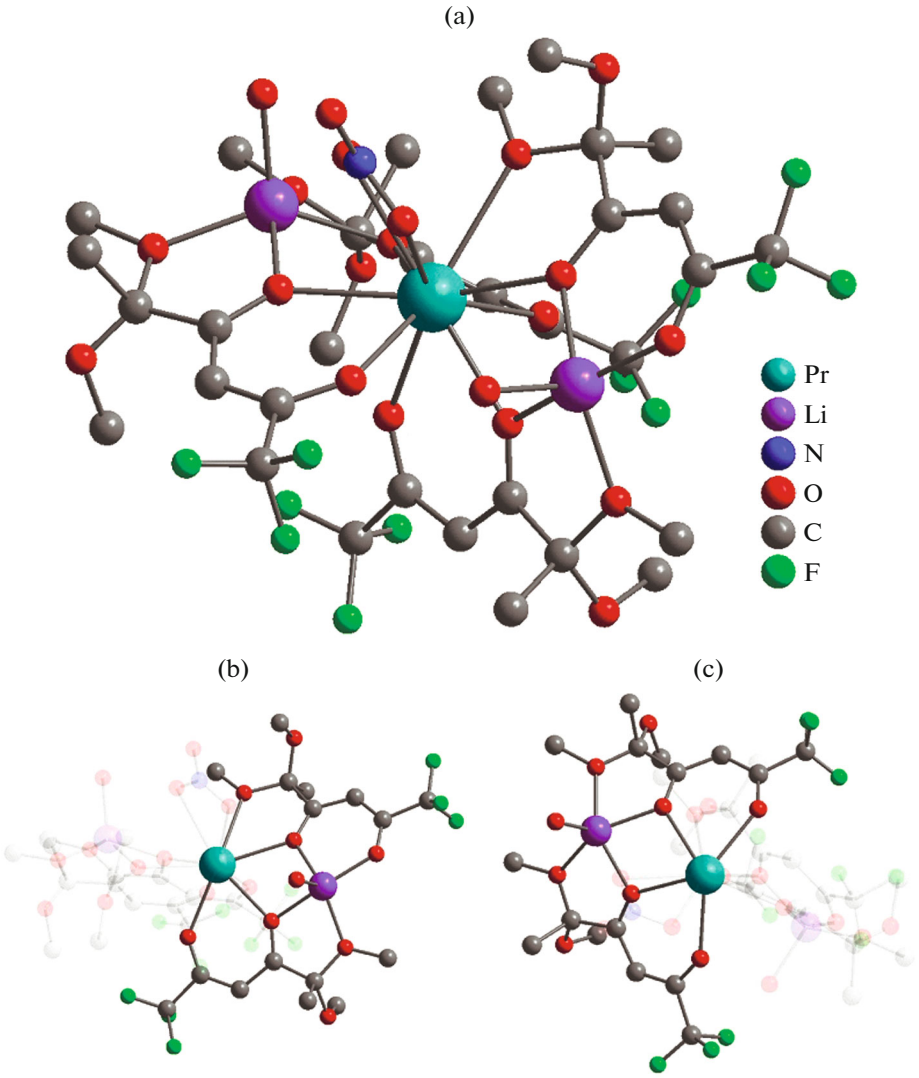

Fig. 4. (a) Molecular structure of complex **II** (hydrogen atoms are omitted), (b) organization of the binuclear Pr–Li fragment involving the ligands from the tris(diketonate) fragment, and (c) organization of the binuclear Pr–Li fragment involving the ligand from the tris(diketonate) fragment and LiL.

between the praseodymium(III) atom and lithium atom of LiL is 3.5704(137) Å (Fig. 4b), and the higher value (3.6388(173) Å) is achieved for the second pair Pr(III)–Li(I) (Fig. 4c). Two lithium ions in complex **II** are additionally coordinated by the water molecules. The geometry of the coordination polyhedron around the praseodymium(III) ion resembles those found for complexes **I*a*** and **I*b*** and corresponds to the clinocrown (Table 2, Fig. 2b). In the crystal packing of compound **II**, the trimetallic frameworks of the molecules are oriented along the *c* axis (Fig. 5).

According to the XRD data, the binuclear heterometallic complexes $[(LnL_3)(LiL)(solv)]$ (**III*a*–III*c*** and **IV*a*–IV*h***) are neutral β-diketonates and crystallize in the space groups $P2_1/c$ and *Pn* of the monoclinic system, respectively (Table 1, Fig. 6). Ethanol turned out to be the most appropriate solvent for the compounds based on praseodymium(III), neodymium(III), and yttrium(III). In the series from Sm(III) to Yb(III), the successful growth of crystals of compounds **IV*a*–IV*h*** was observed in the case of methanol. In complexes **III*a*–III*c*** and **IV*a*–IV*h***, the Ln(III) atom is octacoordinated due to the oxygen atoms of three diketonate anions (coordination mode A) and also due to the methoxy group and bridging oxygen atom of lithium diketonate (coordination mode B) (similarly to Fig. 4b). The lithium atom builds up its coordination environment to $[LiO_5]$ due to the oxygen atoms of two diketonates (coordination modes A and B) and solvent molecules. The water molecule

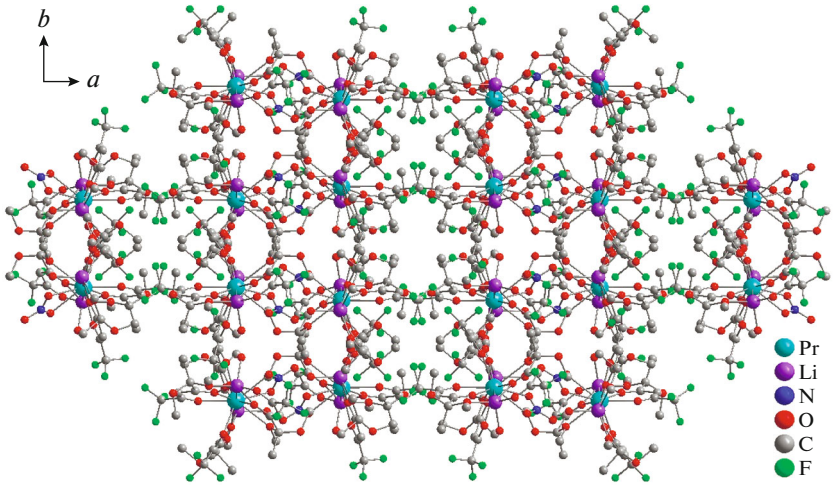

Fig. 5. Crystal packing of complex **II** along the *c* axis (hydrogen atoms are omitted).

acts as a coligand at the lithium atom in compounds **III*a*–III*c***, whereas methanol is the coligand in the cases of compounds **IV*a*–IV*h***.

Complexes **III*a*–III*c*** and **IV*a*–IV*h*** are characterized by similar geometries of the $[LnO_8]$ polyhedron corresponding to a trigonal dodecahedron (Table 2, Fig. 2c). However, these two types of complexes differ by the arrangement of the diketonate anions forming the coordination environment $[LnO_8]$. In the cases of products **III*a*–III*c***, the oxygen atoms (O(5), O(10), and O(15)) of the dicarbonyl fragment adjacent to the trifluoromethyl substituent of the ligands occupy the vertices of two adjacent edges of $[LnO_8]$ (Fig. 7a). Unlike this, in compounds **IV*a*–IV*h*** the similar oxygen atoms (O(4), O(8), and O(13)) occupy one of the polyhedron faces, and three ligand molecules of the Ln(III) tris(diketonate) fragment exist in the cis position relative to each other (Fig. 7b). The arrangement of the different in nature substituents in the dicarbonyl fragment of the ligand around the lanthanide ion affects the crystalline field of the metal and results in changes in the physicochemical properties of the complexes. This is also confirmed by the lifetime of afterflow for $[(LnL_3)(LiL)(MeOH)]$ exceeding those of the corresponding $[(LnL_3)(LiL)(H_2O)]$ complexes (Eu(III), Tb(III), and Dy(III) [25].

Compounds **III*a*–III*c*** and **IV*a*–IV*h*** have different crystal packings (Fig. 8). The water molecules in complexes **III*a*–III*c*** participate in the formation of intermolecular hydrogen bonds, which resulted in approaching the $[LiO_5]$ polyhedra of the molecules and in the formation of zigzag chains along the *b* axis (Fig. 8). In complexes **III*a*–III*c***, the intermolecular Ln...Ln distance is shorter than those in complexes **IV*a*–IV*h*** (Table 2).

It has previously been shown that the study of lanthanide diketonates by ^{19}F NMR spectroscopy gives an important information about the compositions and structures of the complexes in the solution [23, 41–43]. The equilibrium involving three types of metal-containing diketonates according to Scheme 3 (Eq. (1)) has previously been assumed for Ln(III) sodium tetrakis(diketonates) [23, 41, 42]. Another possibility is the coexistence of two isomeric forms of tetrakis(diketonate) in the solution [43].

$$Na[Ln(diketonate)_4] \underset{}{\overset{\text{Deuterated solvent}}{\rightleftharpoons}} Na(diketonate) + Ln(diketonate)_3 \quad (1)$$

$$[(LnL_3)(LiL)] \overset{\text{DMSO-d}_6}{\rightleftharpoons} Li[LnL_4] \quad (2)$$

III*a*, III*b*, IV*b*, IV*d*–*h*

Scheme 3.

It is found that the spectra of homoleptic binuclear diketonates **I*a*** and **I*b*** containing only lanthanide ions exhibit broadened singlet signals of the CF_3 group in the range $\delta_F = 88–89$ ppm, which can be assigned to the bound Ln(III) tris(diketonate) fragments. The chemical shifts of the fluorine atoms for these com-

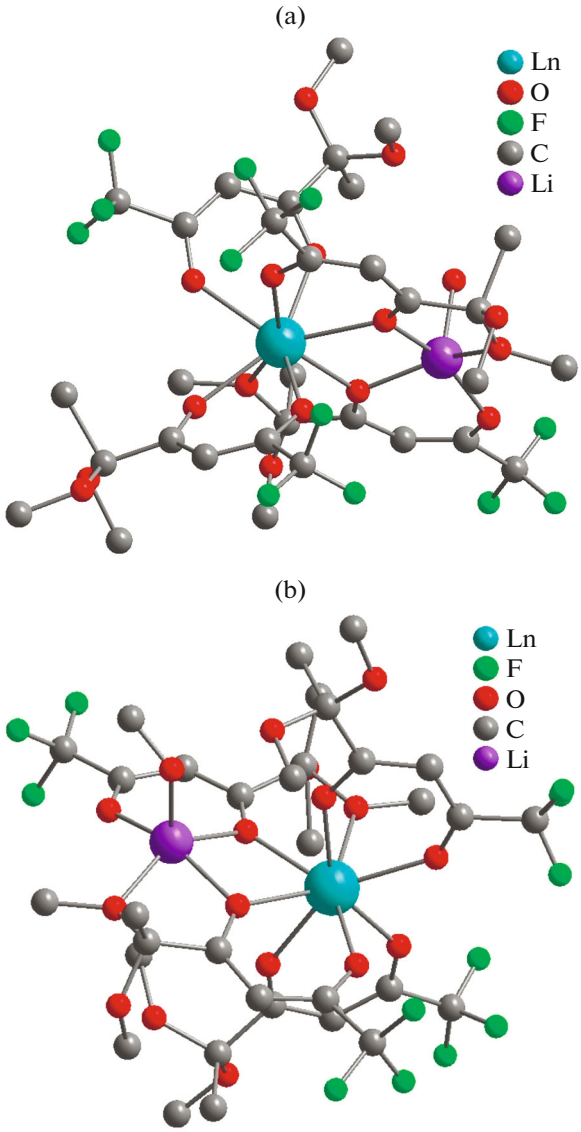

Fig. 6. Molecular structures of complexes (a) **III*a*–III*c*** and (b) **IV*a*–IV*h*** (hydrogen atoms are omitted).

pounds undergo the downfield shift relative to the value of the initial LiL equal to $\delta_F = 87.7$ ppm [30].

All ^{19}F NMR spectra of compounds **II**–**IV** exhibit the lithium diketonate fragment (LiL) at $\delta_F \approx 87.7$ ppm, which is broadened, unlike the spectrum of the LiL salt, indicating that the coordination of the lithium diketonate molecule with the lanthanide fragment is retained in the solution. The distinction in complexes **II**–**IV** is in the set of signals corresponding to the CF_3 groups of the diketonate residues coordinated to Ln(III). Remarkably, the ^{19}F NMR spectra of bi- and trimetallic Pr(III) diketonates **II** and **III*a*** differ by the sets of signals from fluorine atoms and values of chemical shifts. The $[PrL_3]$ fragment is detected at $\delta_F \approx 91.9$ ppm in the case of compound **II**, whereas compound **III*a*** exhibits two signals at $\delta_F = 90.5$ and 91.6 ppm, which can be assigned to the tris and tetrakis forms $[PrL_3]$ and $[PrL_4]$, respectively, existing in the solution. Similarly to complex **II**, one signal of the CF_3 groups corresponding to the tris forms $[LnL_3]$ is observed in the spectra of compounds **III*c***, **IV*a***, and **IV*c***, whereas diketonates $[(LnL_3)(LiL)(solv)]$ (**III*a***, **III*b***, **IV*b***, and **IV*d*–IV*h***) contain the tris form $[LnL_3]$ and tetrakis form $[LnL_4]$. The fluorine atoms of the CF_3 groups of diketonates **III*a*–III*c*** and **IV*a*–IV*c*** bound to the ions from Pr(III) to Gd(III), including yttrium(III), resonate in a higher field at $\delta_F \approx 84$–91 ppm compared to the signals of the group of the Tb(III)–Ho(III) complexes (**IV*d*–IV*g***), which are detected in a lower field and lie in the range $\delta_F \approx 96$–

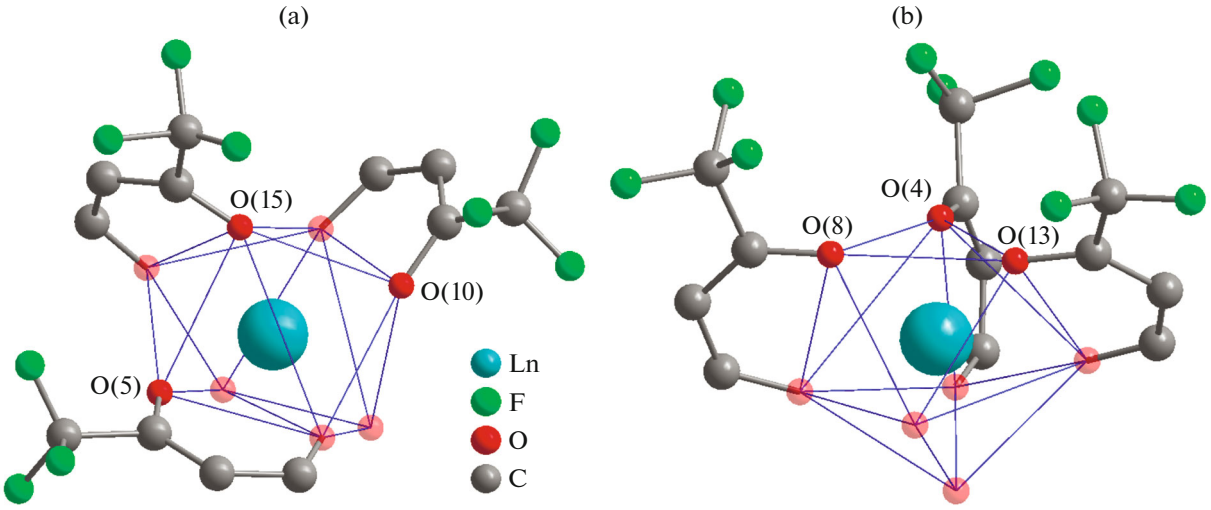

Fig. 7. Arrangement of the ligands in the tris(diketonate) fragment of complexes (a) **III** and (b) **IV**.

120 ppm. Note that the fluorine atoms of complex **IV*c*** corresponding to the CF_3 group of the ligand coordinated to the gadolinium(III) ion give a broadened signal of several ppm. Based on the data obtained, we may conclude that two forms of the majority of lithium–lanthanide complexes **III** and **IV** are equilibrated (Scheme 3, Eq. (2)).

The mass spectra of all complexes are complicated and presented by several ion sequences as cations, where lithium β-diketonate ($C_8H_{10}F_3LiO_4$) plays an important role along with usual protonated ammonium, sodium and potassium forms. Lithium β-diketonate is present in the mass spectra of all compounds by intrinsic sequences of cations in the range of low masses $[nM + Cat]^+$ (n = 1–4) of which the lithium ion (+241.0846 Da) is most intensive and observed in the whole mass spectrum as a difference in masses between different peaks of 234.069 Da. Two types of sequences of the observed ions can be distinguished in the mass spectra, $[LnL_4]^+$ and $[LnL_3]_2^+$, which are additionally accompanied by the ions corresponding to the loss or addition of the ligand and the necessary change in the number of protons, for example, $[LnL_3]^+$, $[(LnL_3)_2 + L]^+$, and $[(LaL_3)_2 - L]^+$. The ions obtained as a result of the loss of the methanol molecules should also be mentioned. The presence of the NO_3 species or water and methanol molecules in complexes **II**–**IV** does not affect the overall view of the mass spectra recorded for solutions in methanol.

For compounds **I**, the signals of the second type $[LnL_3]_2^+$ are weak or absent. The mass spectra of compounds **II**–**IV** are qualitatively resembling, and the ions of the second type can be both intensive and moderately pronounced. Two types of the complexes were obtained for praseodymium: compounds **II** and **III*a***. The mass spectrum of compound **III*a*** (with a lower stoichiometric amount of lithium) contains much more intensive peaks but includes all intensive peaks of the mass spectrum of compound **II**.

It should be mentioned that the full resolution of peaks in the required range is not achieved for a series of compounds because of the insufficient resolution ability of the mass spectrometer used (to 40000). This is due to the fact that a series of polyisotope elements, for example, gadolinium or ytterbium, exhibits a wide distribution over masses of isotopes and because of a large amount of lithium in the sample. As a result, the mass spectrometer detects the signal superposition of impositions of several heteroisotope ions differed in mass from the monoisotope ion by 0.1–1.0 mDa, depending on the metal atom, rather than individual monoisotope ions. Therefore, the experimentally obtained values of ion masses (Fig. 9a) were compared not with the masses of the monoisotope ions but with the calculated values obtained by the simulation calculations at a specified instrumental resolution (Fig. 9b).

To conclude, the reactions of functionalized lithium CF_3-β-diketonate with trivalent REM salts in methanol were shown to afford homo- and heteronuclear lanthanide β-diketonates depending in the metal ion radius. The homoleptic complexes $[LnL_3]$ (**I*a*** and **I*b***) containing two transition metal ions were isolated for lanthanum and cerium. In the case of praseodymium, two types of complexes **II** and **III*a*** were isolated, which is determined by the nature of the anion of the salt. In complexes **I*a***, **I*b***, and **II**, the lanthanide ions

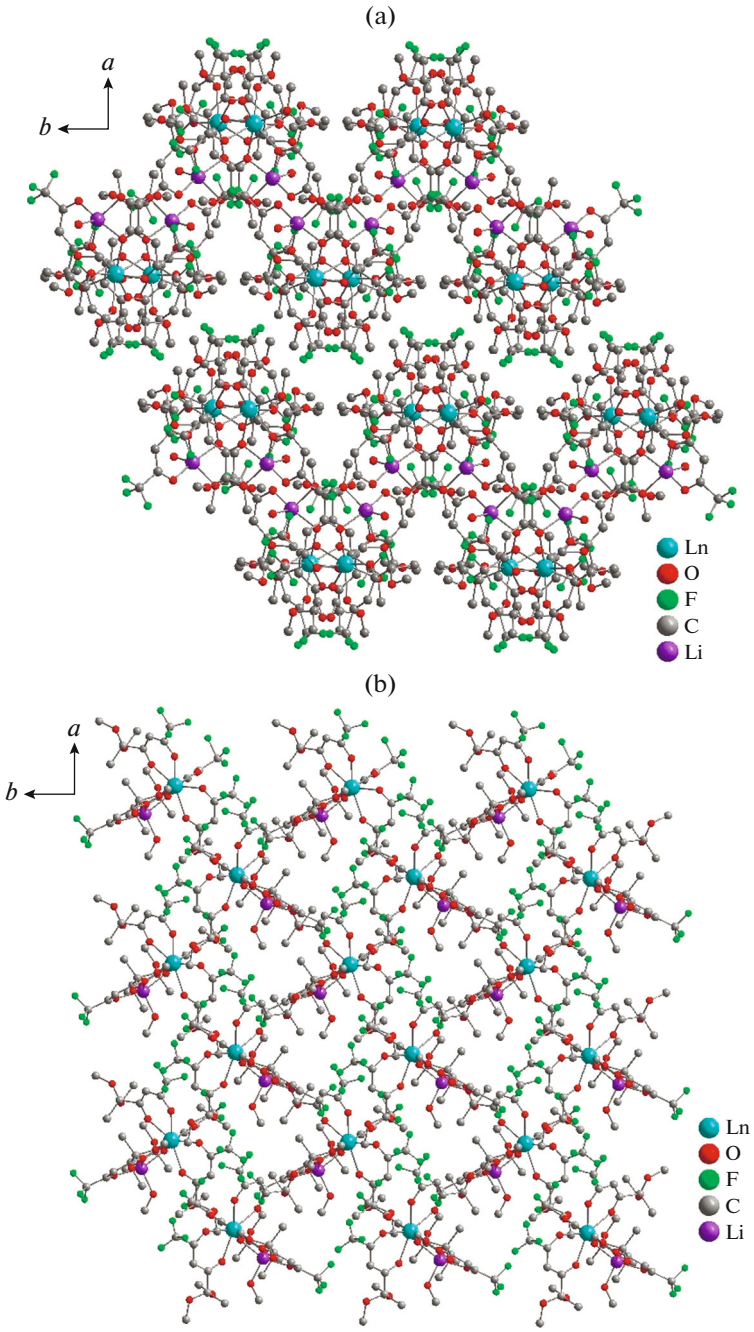

Fig. 8. Crystal packings of complexes (a) **III** and (b) **IV** along the *c* axis (hydrogen atoms are omitted).

are decacoordinated, whereas those for the biheteronuclear complexes $[(LnL_3)(LiL)(solv)]$ (**III*a*–III*c*** and **IV*a*–IV*h***) are octacoordinated. The XRD data show that the acetal group in the ligand structure determines the coordination of the ligand with lithium ions and REM and favors the formation of discrete structures of the bi(tri)metallic complexes.

ACKNOWLEDGMENTS

The XSA and physicochemical studies of the complexes were carried out using the equipment of the Center for Collective Use "Spectroscopy and Analysis of Organic Compounds" at the Postovskii Institute of Organic Synthesis (Ural Branch, Russian Academy of Sciences).

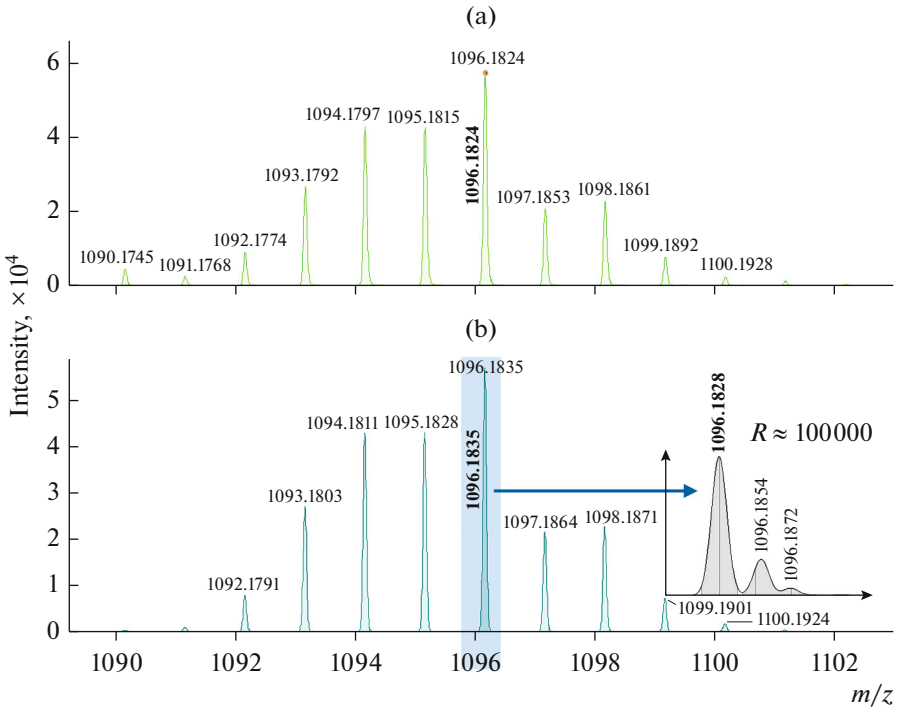

Fig. 9. (a) Experimental mass spectrum of complex **IV*h*** (resolution $R \approx 17000$) and (b) simulation of the mass spectrum of compound **IV*h*** with the calculated (resolution $R \approx 17000$) and expected ($R \approx 100000$) masses of the molecular ion.

FUNDING

This work was supported by the Russian Science Foundation, project no. 19-73-00242.

CONFLICT OF INTEREST

The authors declare that they have no conflicts of interest.

REFERENCES

1. Brock, A.J., Clegg, J.K., Li, F., and Lindoy, L.F., *Coord. Chem. Rev.,* 2018, vol. 375, p. 106.
2. Vigato, P.A., Peruzzo, V., and Tamburini, S., *Coord. Chem. Rev.,* 2009, vol. 253, p. 1099.
3. Condorelli, G.G., Malandrino, G., and Fragala, I.L., *Coord. Chem. Rev.,* 2007, vol. 251, p. 1931.
4. Binnemans, K., *Chem. Rev.,* 2009, vol. 109, p. 4283.
5. Kudyakova, Y.S., Bazhin, D.N., Burgart, Y.V., and Saloutin, V.I., *Mendeleev Commun.,* 2016, vol. 26, p. 54.
6. Pugachev, D.E., Kostryukova, T.S., Ivanovskaya, N.G., et al., *Russ. J. Gen. Chem.*, 2019, vol. 89, p 965.
7. Metlina, D.A., Metlin, M.T., Ambrozevich, S.A., Taydakov, I.V., et al., *J. Lumin.,* 2018, vol. 203, p. 546.
8. Metlin, M.T., Ambrozevich, S.A., Krasnosel'sky, S.S., et al., *Russ. Chem. Bull.,* 2016, vol. 65, p. 1784.
9. Taydakov, I.V., Avetisov, R.I., and Datskevich, N.P., *Russ. J. Coord. Chem.,* 2019, vol. 45, p. 883.
10. Bukvetskii, B.V., Mirochnik, A., and Zhikhareva, P.A., *Luminescence,* 2017, vol. 27, p. 773.
11. Bukvetskii, B.V. and Shishov, A., and Mirochnik, A.G., *Luminescence,* 2016, vol. 31, p. 1329.
12. Fokin, S.V., Ovcharenko, V.I., Romanenko, G.V., et al., *Russ. Chem. Bull.,* 2011, vol. 60, p. 816.
13. Starikov, A.G., Tsaturyan A.A., Starikova A.A., et al., *Russ. Chem. Bull.*, 2018, vol. 67, p. 1182.
14. Artiukhova, N.A., Romanenko, G.V., Letyagin, G.A., et al., *Russ. Chem. Bull.,* 2019, vol. 68, p. 732.
15. Kuznetsova, O.V., Fursova, E.Yu., Letyagin, G.A., et al., *Russ. Chem. Bull.,* 2018, vol. 67, p. 1202.
16. Kuznetsova, O.V., Romanenko, G.V., Bogomyakov, A.S., et al., *Russ. J. Coord. Chem.,* 2020, vol. 46, p. 521.
17. Zhang, T., Pan, J., Duan, J., et al., *ChemCatChem,* 2019, vol. 11, p. 5778.
18. Urkasym kyzy, S., Krisyuk, V.V. Turgambaeva, A.E., et al., *J. Struct. Chem.,* 2019, vol. 60, p. 1635.
19. Peddagopu, N., Rossi, P., Bonaccorso, C., et al., *Dalton Trans.,* 2020, vol. 49, p. 1002.
20. Turgambaeva, A.E., Krisyuk, V.V., Baidina, I.A., et al., *J. Struct. Chem.*, 2017, vol. 58, p. 1530.
21. Urkasym kyzy, S., Shen, H., Mosyagina, S.A., et al., *J. Struct. Chem.*, 2018, vol. 59, p. 433.
22. Lieberman, C.M., Filatov, A.S., Wei, Z., et al., *Chem. Sci.*, 2015, vol. 6, p. 2835.
23. Barry, M.C., Wei, Z., He, T., et al., *J. Am. Chem. Soc.,* 2016, vol. 138, p. 8883.
24. Wei, Z., Han, H., Filatov, A.S., and Dikarev, E.V., *Chem. Sci.*, 2014, vol. 5, p. 813.
25. Bazhin, D.N., Kudyakova, Y.S., Bogomyakov, A.S., et al., *Inorg. Chem. Front.,* 2019, vol. 6, p. 40.

26. Kudyakova, Y.S., Slepukhin, P.A., Valova, M.S., et al., *Russ. J. Coord. Chem.*, 2020, vol. 46, p. 545.
27. Kudyakova, Y.S., Slepukhin, P.A., Valova, M.S., et al., *Eur. J. Inorg. Chem.*, 2020, vol. 2020, p. 523.
28. Krisyuk, V.V., Urkasym Kyzy, S., Rybalova, T.V., et al., *J. Coord. Chem.,* 2018, vol. 71, p. 2194.
29. Bazhin, D.N., Kudyakova, Y.S., Burgart, Y.V., and Saloutin, V.I., *Russ. Chem. Bull.,* 2018, vol. 68, p. 497.
30. Bazhin, D.N., Chizhov, D.L., Röschenthaler, G.-V., et al., *Tetrahedron Lett.,* 2014, vol. 55, p. 5714.
31. Bazhin, D.N., Kudyakova, Y.S., Röschenthaler, G.-V., et al., *Eur. J. Org. Chem.*, 2015, p. 5236.
32. Kudyakova, Y.S., Onoprienko, A.Y., Slepukhin, P.A., et al., *Chem. Heterocycl. Comp.*, 2019, vol. 55, p. 517.
33. Bazhin, D.N., Kudyakova, Y.S., Onoprienko, A.Y., et al., *Chem. Heterocycl. Compd.,* 2017, vol. 53, p. 1324.
34. Bazhin, D.N., Kudyakova, Yu.S., Slepukhin, P.A., et al., *Mend. Commun.,* 2018, vol. 28, p. 202.
35. Dolomanov, O.V., Bourhis, L.J., Gildea, R.J., et al., *J. Appl. Crystallogr.,* 2009, vol. 42, p. 339.
36. Sheldrick, G.M., *Acta Crystallogr., Sect. A: Found. Crystasllogr.,* 2008, vol. 64, p. 112.
37. Casanova, D., Llunell, M., Alemany, P., and Alvarez, S., *Chem.-Eur. J.,* 2005, vol. 11, p. 1479.
38. Llunell, M., Casanova, D., Cirera, J., et al., *SHAPE. Version 2.1*, Barcelona, 2013.
39. YuiKhan, L., Mosyagina, S.A., Stabnikov, P.A., et al., *J. Struct. Chem.*, 2017, vol. 58, p. 843.
40. Shen, H., Berezin, A.S., Antonova, O.V., et al., *J. Struct. Chem.*, 2018, vol. 59, p. 676.
41. Lin, Y., Zou, F., Wan, S., et al., *Dalton Trans.,* 2012, vol. 41, p. 6696.
42. Di Pietro, S. and Di Bari, L., *Inorg. Chem.,* 2012, vol. 51, p. 12007.
43. Monteiro, B., Outis, M., Cruz, H., and Leal, J.P., *Chem. Commun.,* 2017, vol. 53, p. 850.

Translated by E. Yablonskaya